Potential Biological Processes Related to Brain SLC13A5 Across the Lifespan: Weighted Gene Co-Expression Network Analysis from Large Human Transcriptomic Data

Bruna Klippel Ferreira , Patricia Fernanda Schuck , Gustavo Costa Ferreira * , Hércules Rezende Freitas *

Posted Date: 1 January 2026

doi: 10.20944/preprints202601.0041.v1

Keywords: SLC13A5; Na(+)/citrate cotransporter; developmental and epileptic encephalopathy; cerebrum

 doi:10.20944/preprints202601.0041.v1

Article

Potential Biological Processes Related to Brain SLC13A5 Across the Lifespan: Weighted Gene Co-Expression Network Analysis from Large Human Transcriptomic Data

Bruna Klippel Ferreira [1], Patrícia Fernanda Schuck [1], Gustavo Costa Ferreira [1,*] and Hércules Rezende Freitas [2,*]

[1] Laboratório de Erros Inatos do Metabolismo, Programa de Bioquímica e Biofísica Celular, Instituto de Bioquímica Médica Leopoldo de Meis, Universidade Federal do Rio de Janeiro, Rio de Janeiro, Brazil

[2] Laboratório de Informática em Saúde (LabInfoS), Departamento de Ciências Médicas Integradas, Faculdade de Ciências Médicas, Universidade do Estado do Rio de Janeiro, Rio de Janeiro, Brazil

* Correspondence: gustavo.ferreira@bioqmed.ufrj.br (G.C.F.); hercules.freitas@uerj.br (H.R.F.)

Abstract

Background/Objectives: SLC13A5 encodes a sodium–citrate cotransporter implicated in early-onset epileptic encephalopathy and metabolic brain dysfunction, yet its developmental regulation and molecular context in the human brain remain incompletely defined. **Methods:** Leveraging human developmental transcriptomes from the Evo-Devo resource, we delineated tissue trajectories and network context for SLC13A5 across the fetal–postnatal life. **Results:** In the cerebrum, SLC13A5 expression rises from late fetal stages to peak in the first postnatal year and then declines into adulthood, while cerebellar levels increase across the lifespan; liver shows a fetal decrease followed by sustained postnatal upregulation. A transcriptome-wide scan identified extensive positive and negative associations with SLC13A5, and a signed WGCNA built on biweight midcorrelation placed SLC13A5 in a large module. The module eigengene tracked brain maturation (Spearman $\rho = 0.802$, $P = 8.62\times10^{-6}$) and closely matched SLC13A5 abundance ($\rho = 0.884$, $P = 2.73\times10^{-6}$), with a significant partial association after adjusting for developmental rank ($\rho = 0.672$, $P = 6.17\times10^{-4}$). Functional enrichment converged on oxidative phosphorylation and mitochondria. A force-directed subnetwork of the top intramodular members ($|bicor| > 0.6$) positioned SLC13A5 adjacent to a densely connected nucleus including CYP46A1, ITM2B, NRGN, GABRD, FBXO2, CHCHD10, CYSTM1, and MFSD4A. **Conclusions:** Together, these results define a developmentally tuned, mitochondria-centered program that co-varies with SLC13A5 in the human brain across the lifespan. It may provide insights to interrogate age-dependent phenotypes and therapeutic avenues for disorders involving citrate metabolism.

Keywords: SLC13A5; Na(+)/citrate cotransporter; developmental and epileptic encephalopathy; cerebrum

1. Introduction

SLC13A5 epilepsy, also known as developmental epileptic encephalopathy 25 (OMIM # 615905), is an autosomal recessive disease characterized by neonatal seizures, febrile seizures, *status epilepticus*, developmental delay, a severe movement disorder, and lack of tooth enamel. Severe seizures start in the first days of life with better seizure control in late childhood and adolescence but lifelong increased seizure risk [1]. Patients have global developmental delay and impaired motor function [2]. Tooth hypoplasia due to *amelogenesis imperfecta* remains a distinctive feature [3].

 doi:10.20944/preprints202601.0041.v1

To date, more than 50 loss-of-function mutations in human *SLC13A5* have been found to cause SLC13A5 epilepsy [4,5]. Interestingly, there has been no genotype-phenotype correlation identified, though all tested mutations had a severe loss of citrate transporter function [6,7]. *Slc13a5*-knockout mice showed pro-epileptogenic neuronal excitability changes in the hippocampus and approximately 50% of the mice had spontaneous seizures [8].

There are no curative treatments for SLC13A5 epilepsy, and all patients are treated with standard antiseizure medications with mixed results. Previously reported antiseizure medications include benzodiazepines, phenobarbital, phenytoin, and carbamazepine with good seizure control in some patients. However, some patients needed to use up to 10 drugs in polytherapy [1,2]. Although current antiseizure medications may reduce seizure frequency, more targeted treatments are needed to address the epileptic and non-epileptic features of SLC13A5 epilepsy, such as communication and movement disorders [9].

Studies have demonstrated that SLC13A5 epilepsy symptoms change with age [1]. However, it is unknown whether physiological SLC13A5 expression changes over time. The present work is therefore an effort to use large transcriptomic data to investigate SLC13A5 expression in humans.

2. Materials and Methods

2.1. Data Sources

The Evo-Devo application, created by Cardoso-Moreira et al. (2019), is a vast database including expression results for genes in different species, organs, and development stages. Human RNA-seq expression (RPKM) across developmental stages was obtained from the Evo-Devo resource [10]. *SLC13A5* and genome-wide expression for brain and peripheral tissues reported by Evo-Devo were analyzed. Analyses focused on *Homo sapiens* only. Descriptive trajectories were assembled for brain, cerebellum, kidney, liver, testis, and ovary.

2.2. Preprocessing and Sample Ordering

Expression tables were reshaped into sample-by-gene matrices keyed by Ensembl gene identifiers. To stabilize variance, values were transformed as log2(RPKM + 1). Genes with zero variance or entirely missing values were removed, and Ensembl version suffixes were stripped to harmonize identifiers. Brain samples were arranged according to a biologically consistent developmental sequence spanning from 4–20 weeks post-conception through newborn, infant (6 to 9 months old), toddler (2 to 4 years old), school age (7 to 9 years old), teenager (13 to 19 years old), young adult (25 to 32 years old), young mid-age (39 to 41 years old), older mid-age (46 to 54 years old), and senior (58 to 63 years old). Since the Evo–Devo developmental labels are ordinal rather than metrically spaced, an ordinal trait (age rank) was constructed by assigning ranks from 1 to N along this sequence. Data quality was assessed using the WGCNA goodSamplesGenes criterion with a minimum non-missing fraction of 0.30 [11]; only samples and genes passing quality control were retained.

2.3. Transcriptome-Wide Association with SLC13A5

Within the brain data set, transcriptome-wide association was performed across samples, correlating *SLC13A5* (Stable ID: ENSG00000141485) with each expressed gene by using Spearman rank correlation and pairwise handling of missingness. Two-sided P-values were adjusted for multiple testing using Benjamini–Hochberg false discovery rate (FDR). The full correlation landscape was summarized with a volcano-type display and a compact temporal heatmap of the top positively and negatively associated genes to visualize developmental coherence.

 doi:10.20944/preprints202601.0041.v1

2.4. Weighted Gene Co-Expression Network Analysis (WGCNA)

A signed co-expression network was constructed from the brain matrix using biweight midcorrelation (bicor). The soft-thresholding power was chosen from the range 1–20 as the first value achieving a scale-free topology fit $R^2 \geq 0.80$; when no value reached this criterion, a conservative default of 6 was used [12]. Modules were identified with blockwise hierarchical clustering using signed topology overlap, a minimum module size of 30 genes, a merge cut height of 0.25, zero reassignment threshold, and partitioning around medoids respecting the dendrogram [13]. For each module, the first principal component (module eigengene) was computed to summarize expression.

2.5. Module–Trait and Gene–Module Relationships

Associations between the *SLC13A5* module eigengene (SME) and developmental progression were tested using Spearman correlation with the ordinal age group rank. The relationship between SME and *SLC13A5* expression was assessed analogously. A partial Spearman association between SME and *SLC13A5* controlling for age rank was obtained by correlating rank-based residuals from linear models. Intramodular connectivity (kME) was quantified as the signed correlation between each gene and its own module eigengene, providing a continuous measure of hubness.

2.6. Functional Enrichment

Functional enrichment for the *SLC13A5* module was performed while keeping gene-identifier universes consistent with each analysis. Gene Ontology Biological Process testing used Ensembl IDs for both input and background (all genes passing network quality control), with FDR control by Benjamini–Hochberg [14]. KEGG analysis required mapping Ensembl to Entrez Gene identifiers; both the module and the background were mapped symmetrically with deduplication at the Entrez level prior to testing, and FDR was controlled analogously. Transcription-factor target enrichment used MSigDB C3 TFT signatures retrieved via msigdbr [15], tested as over-representation on HUGO Gene Nomenclature Committee (HGNC) symbols with a matching symbol-level background. Enrichment results were summarized by −log10(FDR) and gene-ratio for the most significant terms.

2.7. Co-Expression Subnetwork Visualization

To illustrate intramodular organization, the 30 genes with the highest absolute kME within the *SLC13A5* module were selected, with *SLC13A5* forcibly included (if not originally among the top 30). Pairwise bicor values were computed within this set, and an undirected edge was drawn when the absolute correlation exceeded 0.60 [16]. The graph was laid out with a Fruchterman–Reingold force-directed algorithm using a fixed random seed for reproducibility. Node size and color encode |kME|, labels are shown for *SLC13A5* and the highest-connectivity genes, and edges incident to *SLC13A5* are highlighted to delineate its immediate neighborhood.

2.8. Statistical Considerations

Since expression distributions deviated substantially from normality, nonparametric measures, such as Spearman's rho (ρ), were used throughout for association. All tests were two-sided, and multiplicity was controlled by Benjamini–Hochberg FDR unless otherwise stated. Random seeds were fixed where stochastic procedures were involved to ensure reproducibility of visual layouts and summaries. All analyses were performed using the R language (version 4.5.1) with the IDE RStudio (version 2025.9.1.401). A reproducible script is provided as supplementary material.

3. Results

To determine SLC13A5 expression across tissues and how expression changes throughout development, we analyzed SLC13A5 expression using the human data from Cardoso-Moreira et al. (2019). Figure 1 shows the longitudinal view of SLC13A5 expression in different human tissues,

 doi:10.20944/preprints202601.0041.v1

namely cerebrum (Figure 1A), cerebellum (Figure 1B), liver (Figure 1C), kidney (Figure 1D), testis (Figure 1E), and ovaries (Figure 1F). Mean values for pre- and post-conception SLC13A5 expression (RPKM) by tissue are shown in Table 1.

Table 1. Pre- and post-conception *SLC13A5* expression (RPKM) by tissue.

		Conception Stage					
Tissue	**N**	**Overall** (N=26)[1]	**Pre** (N=14) [1]	**Post** (N=12) [1]	**Diff.** [2]	**95% CI** [2]	***p*-Value** [2]
Cerebrum	22	0.7 ± 0.9	0.2 ± 0.1	1.4 ± 1.1	-1.2	-2.1, -0.40	0.009
Cerebellum	20	0.5 ± 0.4	0.3 ± 0.3	0.7 ± 0.3	-0.39	-0.69, -0.09	0.015
Heart	19	0.1 ± 0.1	0.0 ± 0.1	0.1 ± 0.1	-0.01	-0.12, 0.09	0.8
Kidney	18	0.2 ± 0.2	0.2 ± 0.2	0.1 ± 0.1	0.08	-0.08, 0.24	0.3
Liver	22	46.9 ± 14.2	43.5 ± 10.3	53.0 ± 18.6	-9.5	-26, 6.4	0.2
Ovary	12	0.4 ± 0.2	0.4 ± 0.2	-	-	-	-
Testis	21	0.4 ± 0.3	0.4 ± 0.2	0.4 ± 0.3	-0.08	-0.33, 0.18	0.5

[1] Mean ± SD

[2] Welch Two Sample *t*-test; NA

Abbreviation: CI = Confidence Interval

 doi:10.20944/preprints202601.0041.v1

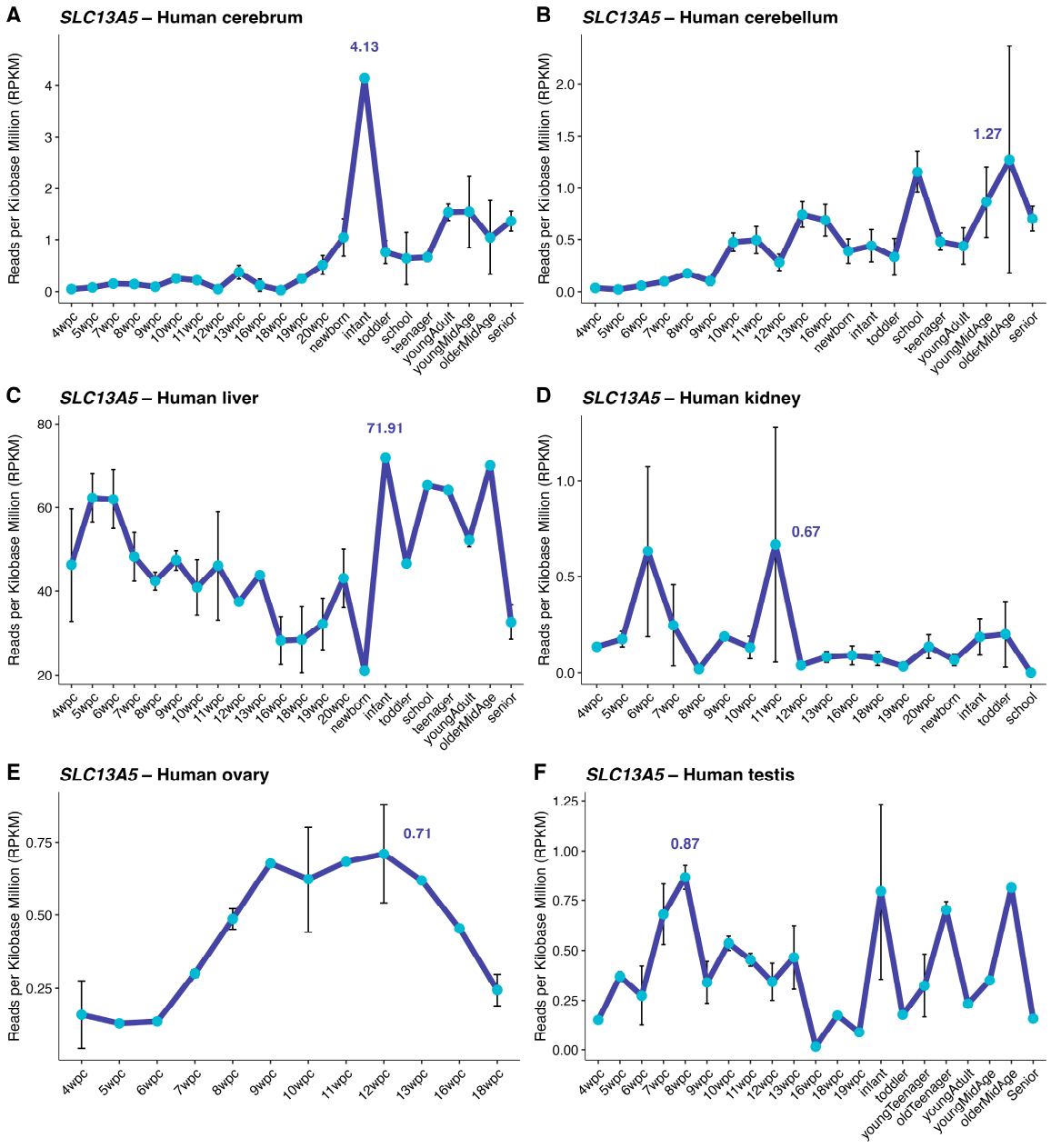

Figure 1. *SLC13A5* expression in human central and peripheral tissues. RPKM for *SLC13A5* expression is shown at different age categories for (**A**) Cerebrum, (**B**) Cerebellum, (**C**) Liver, (**D**) Kidney, (**E**) Ovary, and (**F**) Testis. Each panel depicts the biological ordering from fetal weeks post-conception through postnatal stages, with the within-tissue median ± IQR annotated. Data are expressed as mean RPKM ± SEM.

In the cerebrum, *SLC13A5* expression increases from ~0.5 RPKM at 19 weeks post-conception (WPC) to ~4 RPKM in the first year of life. This is followed by a decrease in cerebrum *SLC13A5* expression until adult life, when levels are kept above 1 RPKM for the following decades. In early stages of development, cerebellar *SLC13A5* expression is less than 1 RPKM (0.3 ± 0.3 RPKM) but increases slowly and continuously throughout life (0.7 ± 0.3 RPKM). Liver is the tissue with the highest *SLC13A5* expression. Following an initial drop during the fetal period until birth (from ~50 RPKM to ~20 RPKM), *SLC13A5* expression increases and is kept high (~60 RPKM) until the end of adulthood. Other peripheral tissues (including kidney, ovaries, and testis) are also low throughout life.

We then assessed the genes whose expression co-varies with *SLC13A5* across development in the human cerebrum transcriptome. A transcriptome-wide correlation scan across Evo-Devo

 doi:10.20944/preprints202601.0041.v1

cerebrum samples revealed extensive bidirectional associations with *SLC13A5* expression (Figure 2A). It includes both positively and negatively correlated genes after multiple-testing correction. To examine whether these relationships are developmentally organized, we evaluated z-scored expression for the top *SLC13A5*-correlated genes across fetal-to-postnatal stages. The heat map shows temporal coherence, with many transcripts mirroring the fetal-to-postnatal shift observed for *SLC13A5* (Figure 2B). Over-representation analyses of this set of genes flagged processes/pathways linked to mitochondrial energy metabolism (notably oxidative phosphorylation), RNA processing and surveillance (including spliceosome-related terms), and cell-cycle/chromatin regulation (Figure 2C–D).

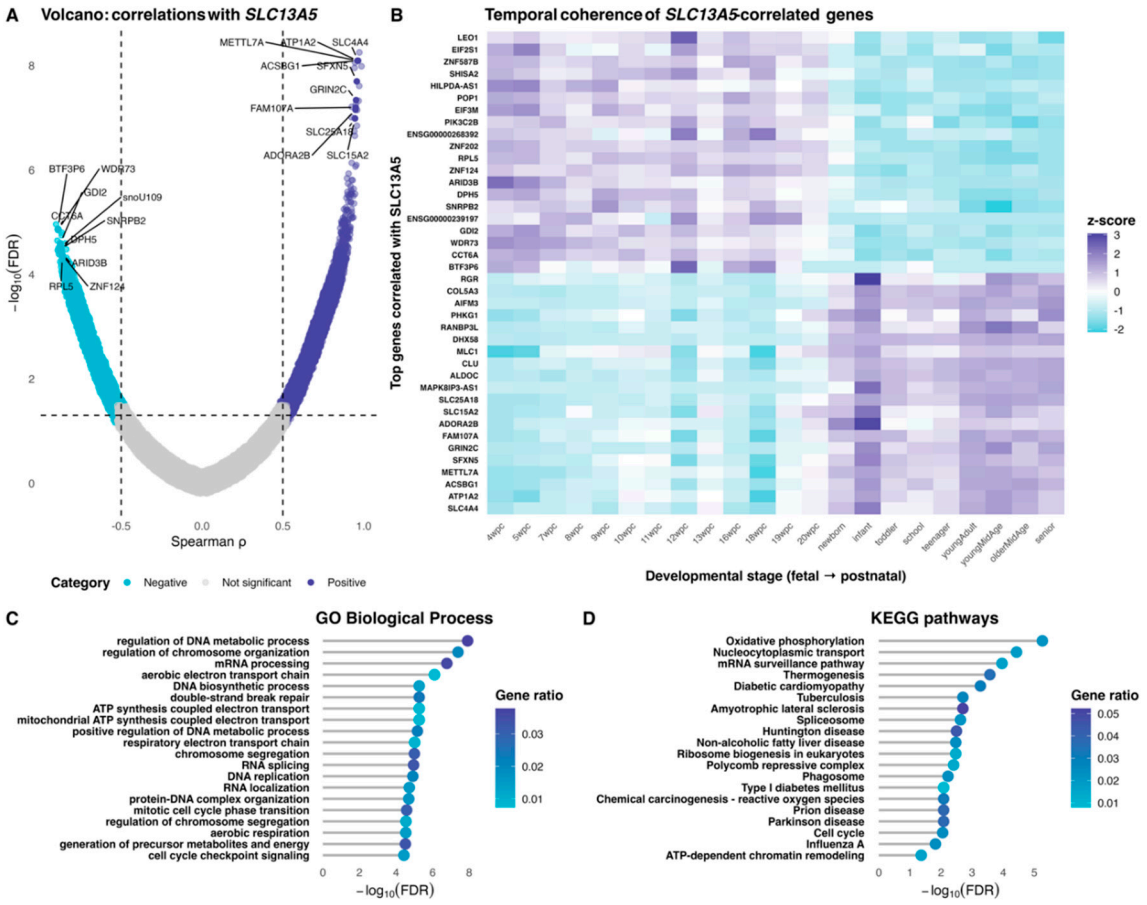

Figure 2. Transcriptome-wide association landscape for SLC13A5 in the human cerebrum. (**Panel A**) shows a volcano-type display of Spearman correlations between *SLC13A5* and all expressed genes across cerebrum samples (dashed guides at ϱ = ±0.5 and at the Benjamini–Hochberg FDR = 0.05 threshold). Labeled points indicate the most significant positive and negative associates after FDR correction. (**Panel B**) presents a compact heat map of the top positively and negatively associated genes (at all developmental stages from 4 wpc to senior), showing z-scored expression to emphasize temporal gradient. (**Panels C,D**) summarize functional enrichment among FDR-significant correlates: **C** Gene Ontology Biological Process using Ensembl identifiers for *SLC13A5*-correlated genes; (**D**) KEGG pathways using a symmetric Ensembl→Entrez mapping. The color of the dots indicates the gene ratio. The y-axis reflects −log10(FDR), with terms ranked by significance.

Network construction of the human cerebrum yielded a scale-free–like topology at low double-digit soft thresholds, with the signed bicor fit approaching the conventional R2 = 0.8 plateau and remaining stable thereafter (Figure 3A). Using this parameter, WGCNA identified a heterogeneous module landscape with a few very large groups and many smaller ones (Figure 3B); the “grey” set aggregated unassigned genes, while the turquoise and blue modules comprised the largest structured clusters. The hierarchical dendrogram revealed block structure (Figure 3C). The aligned annotation tracks (Figure 3D) showed that *SLC13A5* is found in the turquoise module, where genes with the

 doi:10.20944/preprints202601.0041.v1

strongest gene significance to *SLC13A5* (red in GS track) spatially co-localize with high intramodular connectivity (deep red in |kME| track).

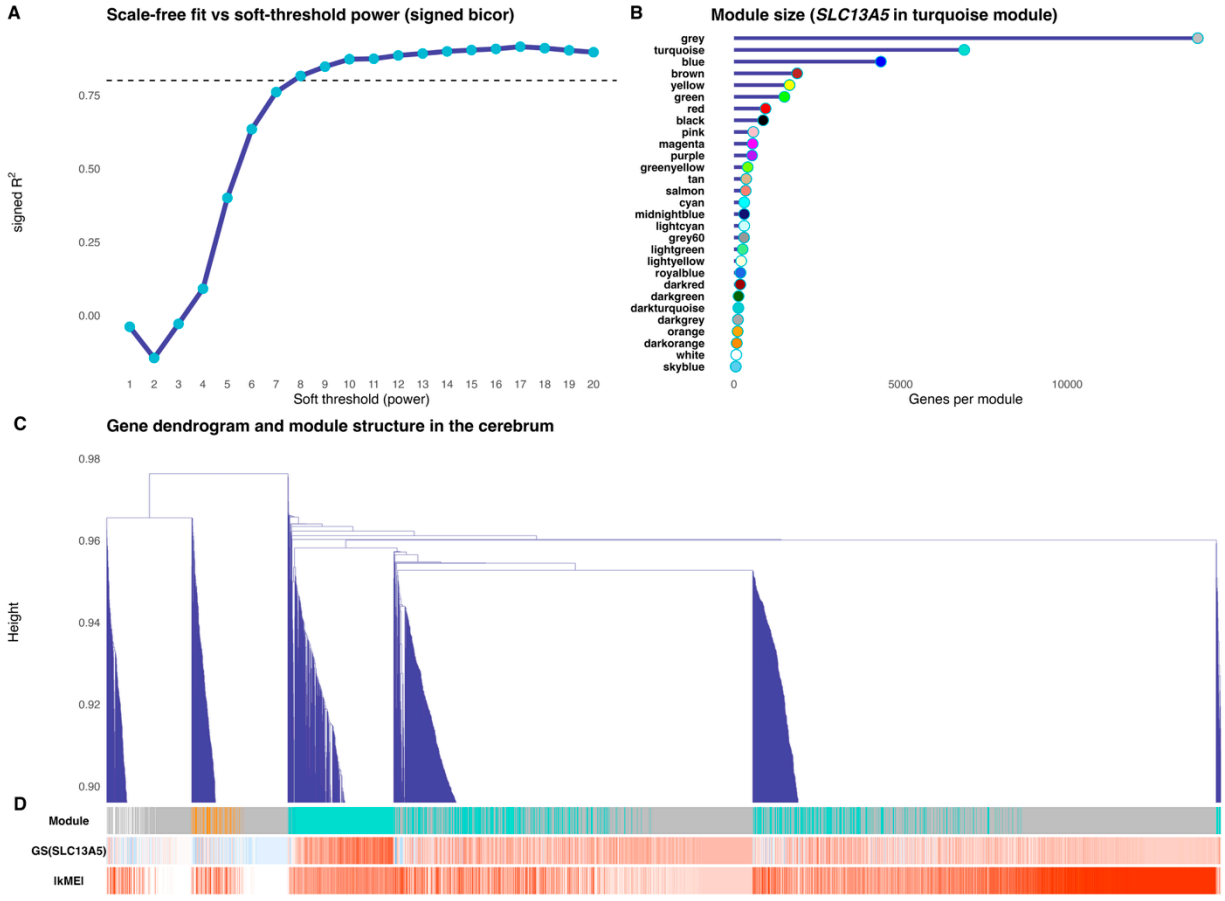

Figure 3. Network architecture of the cerebrum co-expression map. (**Panel A**) displays the scale-free topology fit versus soft-thresholding power for a signed, bicor network; the chosen power corresponds to the first value achieving $R^2 \geq 0.80$ (fallback applied when no value reaches the criterion). (**Panel B**) shows module size distribution (genes per module), with the circle color fill matching the WGCNA module color key used throughout. (**Panels C,D)** show the gene dendrogram with aligned color tracks: **C** the dendrogram is zoomed at the top to emphasize branch topology; **D** annotation bars reporting, in order, module assignment (module colors), gene significance to *SLC13A5* (bicor with *SLC13A5*; blue[high]-white-red[low]), and intramodular connectivity (|kME|; blue[high]-white-red gradient[low]).

The *SLC13A5* module's eigengene tracked cerebrum maturation and the gene's own expression (Figure 4). Across fetal-to-postnatal stages, the eigengene rose in accordance with developmental rank (Spearman $\rho = 0.802$, $P = 8.62 \times 10^{-6}$; Figure 4A), indicating that the turquoise module is progressively activated during human cerebrum development. The eigengene was also tightly correlated with *SLC13A5* expression itself ($\rho = 0.884$, $P = 2.73 \times 10^{-6}$; Figure 4B), consistent with *SLC13A5* being embedded within, and representative of, the module. Importantly, this association persisted after regressing out age effects: a partial correlation between the eigengene and *SLC13A5* (controlling for developmental rank) remained significant ($\rho = 0.672$, $P = 6.17 \times 10^{-4}$; Figure 4C).

 doi:10.20944/preprints202601.0041.v1

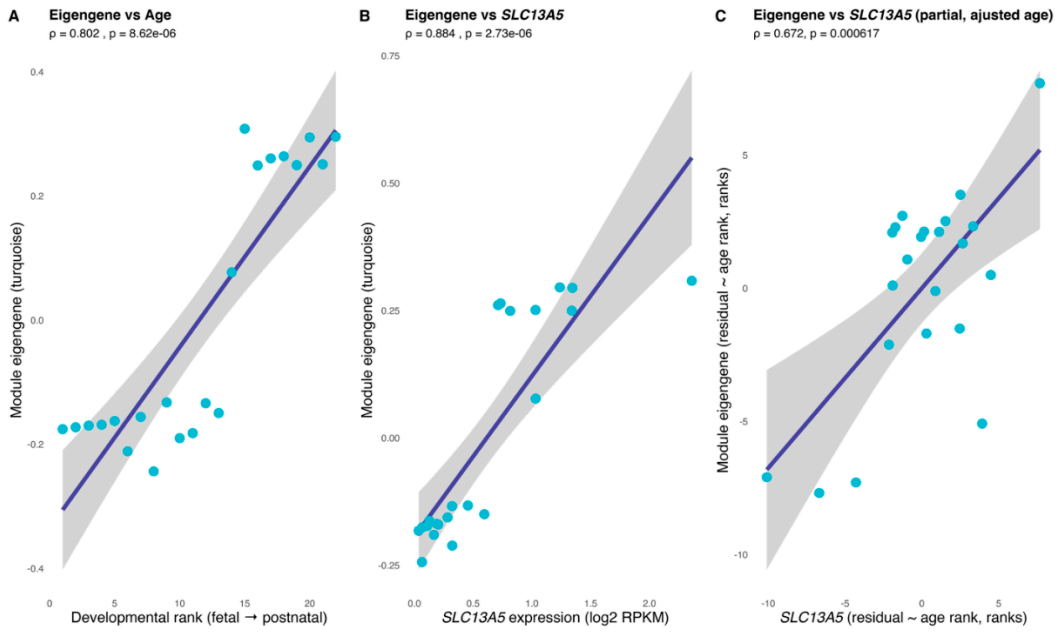

Figure 4. The *SLC13A5* module tracks neurodevelopment and the gene itself. (**Panel A**) shows the association between the *SLC13A5* module eigengene (SME) and the ordinal developmental rank (age rank) across cerebrum samples. (**Panel B**) depicts the association between SME and *SLC13A5* expression (log2-transformed). A partial Spearman correlation controlling for age rank (computed on rank-based residuals) is provided in the (**panel C**). Spearman ϱ and two-sided P are indicated in all panels.

To visualize the local wiring of the *SLC13A5* module, a force-directed subnetwork composed of the top 30 module members was plotted (ranked by |kME|); edges represent robust pairwise co-expression (|bicor| > 0.6) (Figure 5). The layout reveals a compact nucleus of highly interconnected genes with high module cohesion, flanked by a few peripheral nodes with weaker within-module connectivity. *SLC13A5* sits adjacent to the core and forms numerous strong links to neuronal and mitochondrial/transport genes (including *CYP46A1, ITM2B, NRGN, GABRD, FBXO2, CHCHD10, CYSTM1, MFSD4A, CORO6,* and *LYNX1*), consistent with the functional enrichments for oxidative metabolism, RNA/protein homeostasis and synaptic programs. In contrast, nodes such as *ABCC3, CRACDL,* and *TUBA4A* occupy a more peripheral position with fewer edges, indicating lower intramodular connectivity.

 doi:10.20944/preprints202601.0041.v1

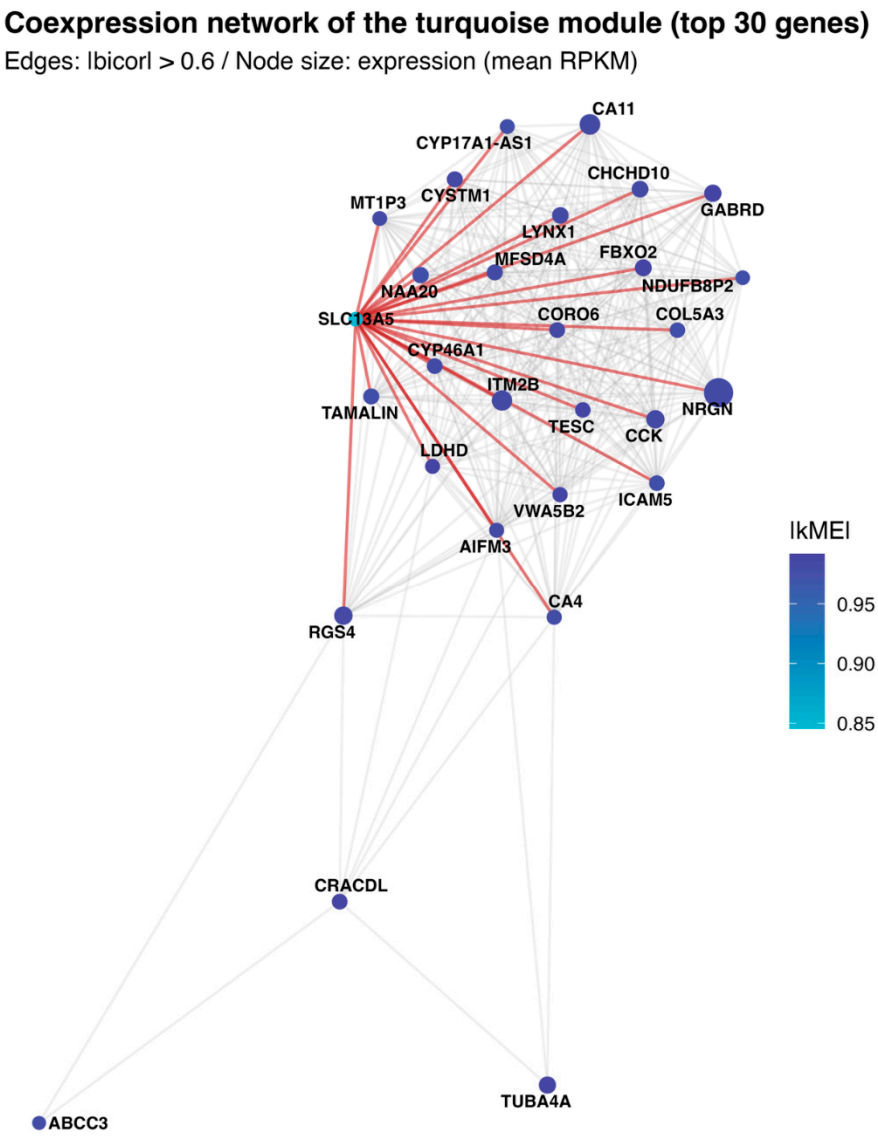

Figure 5. Intramodular co-expression network linked to *SLC13A5*. A force-directed graph depicts the top 30 genes by absolute intramodular connectivity (|kME|) within the *SLC13A5* module, with *SLC13A5* forcibly included when necessary. Undirected edges connect pairs with |bicor| > 0.60, emphasizing robust associations. Node color encodes |kME|, size represents cerebrum gene expression (mean RPKM); labels are shown for *SLC13A5* and the highest-connectivity nodes. Edges incident to *SLC13A5* are highlighted (in red) to delineate its immediate neighborhood within the module.

Gene set enrichment of the *SLC13A5*-containing module revealed a coherent, mitochondria-centered program (Figure 6). In GO Biological Process (panel A), top terms were related to mitochondrial metabolism, including ‘aerobic electron transport chain’, ‘respiratory electron transport chain’, ‘ATP synthesis coupled electron transport’, and ‘mitochondrial ATP synthesis coupled electron transport’. Other terms also revealed involvement with inflammation and purine metabolism. KEGG analysis (panel B) showed a significant enrichment for ‘oxidative phosphorylation’ and pathways involved in neurodegenerative and inflammatory diseases. Transcription-factor–target enrichment (MSigDB C3 TFT; panel C) highlighted regulators consistent with these themes, including NFE2/NRF-like motifs, TFAM-associated genes and AP-1 family targets (multiple AP1 motif sets), as well as ELF1/BACH2 target sets.

 doi:10.20944/preprints202601.0041.v1

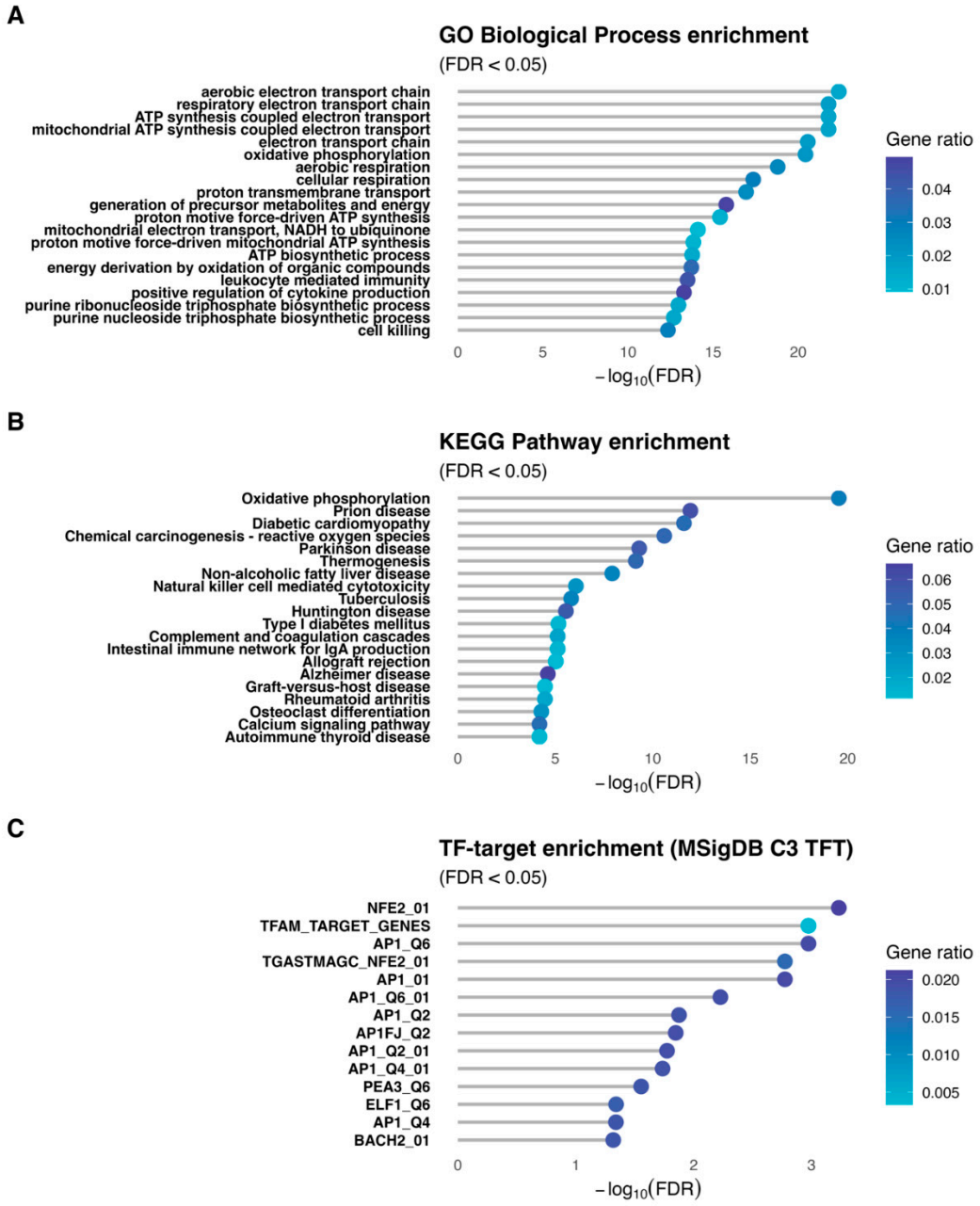

Figure 6. Functional programs enriched in the SLC13A5 module. Gene-set over-representation for the *SLC13A5* module is shown for Gene Ontology Biological Process (**Panel A**), KEGG pathways (**Panel B**), and MSigDB C3 transcription-factor targets (**Panel C**). Universes are matched to each test (all network-tested genes in Ensembl for GO; symmetric Ensembl→Entrez mapping for KEGG; symbol-level background for TF targets). Points encode the gene ratio by color, and the y-axis indicates −log10(FDR). Displayed terms are the top results by FDR, highlighting processes and pathways linked to the module's coordinated variation.

4. Discussion

SLC13A5 plays a key role in citrate metabolism, impacting on hepatic lipogenesis, cell proliferation, bone development, and epilepsy in mammals [17]. Loss-of-function mutations in the *SLC13A5* gene have been associated with SLC13A5 epilepsy [18]. On the other hand, overexpression of *Slc13a5* in neurons from mouse forebrain has been linked to disrupted white matter integrity and autistic-like behaviors [19]. *Slc13a5* overexpression also causes progeria-like phenotype, systemic

 doi:10.20944/preprints202601.0041.v1

inflammation, and alterations in protein acetylation [20]. Thus, SLC13A5 may present different roles/importance across lifespan.

The physiological pattern of *SLC13A5* expression across life in human tissues has not been described yet. We then used a dataset of human tissues from Moreira and colleagues (2019) to start addressing this issue. Liver was the tissue with higher *SLC13A5* mRNA expression at all timepoints investigated. Previous reports showed *SLC13A5* expression much higher in liver than in brain (for both humans and rats) [21,22]. In cerebrum, *SLC13A5* mRNA expression increased from conception until infancy, when it reaches its peak. An increase in *Slc13a5* mRNA expression during early postnatal life was also shown in rat cerebral cortex [23]. Cerebellar expression of SLC13A5 steadily increased throughout life. *Slc13a5*-knockout mice show distinct metabolic pathways disrupted depending on the tissue investigated [24]. Thus, the distinct patterns of *SLC13A5* mRNA expression reported here may cooperate to the different roles played by SLC13A5 in the metabolism of these tissues.

We then assessed expression data of all cerebrum genes in the Evo-Devo database and ran multiple Spearman correlation analyses against the longitudinal expression of *SLC13A5*. We found sets of genes with strong correlation (positive or negative) and time coherence appropriateness with *SLC13A5* expression. Analysis of gene ontology and KEGG pathways indicate that SLC13A5 sits in a developmentally coherent gene neighborhood enriched for mitochondrial bioenergetics and gene-regulatory pathways in the human cerebrum. Genes related to transcription, translation, and synthesis of proteins are critical during neurodevelopment, and dysfunction of these genes may cause reduced brain volume, developmental delay, cognitive deficits, alterations in neural cristae, and neuronal alteration [25–28]. Additionally, the tuning of bioenergetic metabolism is crucial during neurodevelopment. Shifts in bioenergetics control cell fate, as well as neural progenitor proliferation and differentiation [29].

In order to evaluate the network hierarchy, we performed a weighted gene co-expression network analysis and evaluated the intramodular connectivity. The results of WGCNA validated the chosen network parameters, delineated the global co-expression architecture of the developing brain, and defined a densely connected *SLC13A5*-centered module for downstream analyses. The analyses of association between SLC13A5, the eigengene, and developmental rank indicated that the module captures a coordinated expression program that matches developmental progression and specifically co-varies with *SLC13A5* (regardless of the global age trajectory).

The analysis of |kME| within the *SLC13A5* module suggested that *SLC13A5* is embedded in a densely connected module. It is directly connected to genes involved in neuronal homeostasis (synaptic signaling and structural proteins), mitochondrial organization, and lipid/cholesterol turnover. It is feasible that SLC13A5 plays a role in the cooperation between brain and liver for citrate homeostasis, maintaining lipid balance throughout the body (including basic and complex lipids) [24]. We also observed the presence of genes important for calcium handling (e.g., *NRGN* and *TESC*) [30–32] for cell signaling, metabolism, and fate (e.g., *CYP46A1, LDHD, CA4, CA11, RGS4, CHCHD10, AIFM3* and *TAMALIN*) [33–39] as well as cell structure and extracellular matrix (e.g., *COL5A3, ICAM5, TUBA4A* and *CORO6*) [40–43]. Interestingly, *GABRD* was found directly connected to *SLC13A5* in the module. *GABRD* is a gene that encodes GABAA subunit, an important receptor during neurodevelopment and for epilepsy [44]. SLC13A5 was also directly connected to *LYNX1*, a gene encoding a protein that modulates nAChR. Alterations in nAChR are associated with some epilepsies [45]. *LYNX1* dysregulation was reported in Fragile X Syndrome, a condition characterized by epilepsy [46], and in neurodevelopmental disorders [47]. Additionally, knockout of *Lynx1* in animal models enhances synaptic efficacy and performance in memory tests. However, it induces neurodegeneration by the hyperactivation of nAChR [48].

The functional programs enriched in the *SLC13A5* module were then analyzed. GO Biological Process enrichment analysis indicated that the *SLC13A5* module is embedded in a developmental program with genes involved in mitochondrial energy metabolism, reflecting a transcriptional coordination between mitochondrial homeostasis and *SLC13A5*. KEGG analysis showed an

 doi:10.20944/preprints202601.0041.v1

enrichment in pathways associated with neurodegenerative disease (Parkinson's, Alzheimer's, Huntington's disease) and metabolic and inflammatory diseases (type I diabetes, non-alcoholic fatty liver disease, rheumatoid arthritis). Interestingly, SLC13A5 inhibition has also been suggested as a potential therapeutic target for kidney disease [49], hyperlipidemia [50], non-alcoholic fatty liver disease, insulin resistance, and a myriad of metabolic diseases [51–54]. The underlying mechanisms may involve decreasing citrate uptake from blood and reducing intracellular levels of citrate in the liver [55]. The enriched transcription-factor targets include factors such as NFE2, TFAM, and members of the AP-1 family (API, AP1F), implicated in the regulation of mitochondrial biogenesis, stress response, and cell differentiation [40,56–58]. The presence of TFAM, a key regulator of mitochondrial transcription, is particularly relevant. Altogether, the data suggest that this module may represent a regulatory axis relevant to physiological and pathophysiological conditions involving mitochondria.

5. Conclusions

SLC13A5 is highly expressed in the brain in the first years of life, suggesting an important role in this period of life and coinciding with the onset of seizures in SLC13A5 patients. Potential targets of metabolic interplay with SLC13A5 include mitochondria, neurotransmission-related genes, and lipid metabolism. These findings deepen our understanding of the *SLC13A5* expression patterns and highlight its potential significance in cellular metabolism and disease pathogenesis. Continued investigation into the molecular mechanisms underlying SLC13A5 regulation and its functional implications in health and disease will be essential for unraveling its full biological significance and therapeutic potential. For instance, a better understanding of the mechanisms behind age- and tissue-specific *SLC13A5* transcription would help identify targeted therapeutics for SLC13A5 epilepsy and other metabolic disorders with altered citrate homeostasis. Future studies should also investigate neurotransmitter changes after loss of SLC13A5 to elucidate the functional role of SLC13A5 in neurotransmission.

Supplementary Materials: The following supporting information can be downloaded at the website of this paper posted on Preprint.org.

Author Contributions: Conceptualization, BKF, PFS, GCF and HRF; methodology, HRF; software, HRF; formal analysis, BKF, PFS, GCF and HRF; data curation, HRF; writing—original draft preparation, BKF and HRF; writing—review and editing, BKF, PFS, GCF and HRF; supervision, PFS, GCF and HRF; project administration, PFS and GCF; funding acquisition, BKF, PFS, GCF and HRF. All authors have read and agreed to the published version of the manuscript.

Data Availability Statement: The raw data supporting the conclusions of this article will be made available by the authors upon reasonable request.

Acknowledgments: This work was supported by the Carlos Chagas Filho Research Support Foundation of the State of Rio de Janeiro (FAPERJ, Brazil) and the National Council for Scientific and Technological Development (CNPq, Brazil). HRF was supported by the 2024/2025 Coimbra Group Scholarship Programme for Young Professors and Researchers from Latin American Universities, as well as the Tess Research Foundation (TRF, USA) Early-Career Investigator Research Grant, 2022/2023.

Conflicts of Interest: The authors declare that the research was conducted in the absence of any commercial or financial relationships that could be construed as a potential conflict of interest.

References

1. Matricardi, S.; De Liso, P.; Freri, E.; Costa, P.; Castellotti, B.; Magri, S.; Gellera, C.; Granata, T.; Musante, L.; Lesca, G.; et al. Neonatal Developmental and Epileptic Encephalopathy Due to Autosomal Recessive Variants in SLC13A5 Gene. *Epilepsia* **2020**, *61*, 2474–2485, doi:10.1111/epi.16699.

 doi:10.20944/preprints202601.0041.v1

2. Spelbrink, E.M.; Brown, T.L.; Brimble, E.; Blanco, K.A.; Nye, K.L.; Porter, B.E. Characterizing a Rare Neurogenetic Disease, SLC13A5 Citrate Transporter Disorder, Utilizing Clinical Data in a Cloud-Based Medical Record Collection System. *Front. Genet.* **2023**, *14*, doi:10.3389/fgene.2023.1109547.
3. Hardies, K.; de Kovel, C.G.F.; Weckhuysen, S.; Asselbergh, B.; Geuens, T.; Deconinck, T.; Azmi, A.; May, P.; Brilstra, E.; Becker, F.; et al. Recessive Mutations in SLC13A5 Result in a Loss of Citrate Transport and Cause Neonatal Epilepsy, Developmental Delay and Teeth Hypoplasia. *Brain* **2015**, *138*, 3238–3250, doi:10.1093/brain/awv263.
4. Brown, T.L.; Bainbridge, M.N.; Zahn, G.; Nye, K.L.; Porter, B.E. The Growing Research Toolbox for SLC13A5 Citrate Transporter Disorder: A Rare Disease with Animal Models, Cell Lines, an Ongoing Natural History Study and an Engaged Patient Advocacy Organization. *Ther Adv Rare Dis* **2024**, *5*, 26330040241263972, doi:10.1177/26330040241263972.
5. Goodspeed, K.; Liu, J.S.; Nye, K.L.; Prasad, S.; Sadhu, C.; Tavakkoli, F.; Bilder, D.A.; Minassian, B.A.; Bailey, R.M. SLC13A5 Deficiency Disorder: From Genetics to Gene Therapy. *Genes* **2022**, *13*, 1655, doi:10.3390/genes13091655.
6. Klotz, J.; Porter, B.E.; Colas, C.; Schlessinger, A.; Pajor, A.M. Mutations in the Na+/Citrate Cotransporter NaCT (SLC13A5) in Pediatric Patients with Epilepsy and Developmental Delay. *Mol Med* **2016**, *22*, 310–321, doi:10.2119/molmed.2016.00077.
7. Wang, W.-A.; Ferrada, E.; Klimek, C.; Osthushenrich, T.; MacNamara, A.; Wiedmer, T.; Superti-Furga, G. Large-Scale Experimental Assessment of Variant Effects on the Structure and Function of the Citrate Transporter SLC13A5. *Sci Adv* **2025**, *11*, eadx3011, doi:10.1126/sciadv.adx3011.
8. Henke, C.; Töllner, K.; van Dijk, R.M.; Miljanovic, N.; Cordes, T.; Twele, F.; Bröer, S.; Ziesak, V.; Rohde, M.; Hauck, S.M.; et al. Disruption of the Sodium-Dependent Citrate Transporter SLC13A5 in Mice Causes Alterations in Brain Citrate Levels and Neuronal Network Excitability in the Hippocampus. *Neurobiol Dis* **2020**, *143*, 105018, doi:10.1016/j.nbd.2020.105018.
9. Ozlu, C.; Adams, R.M.; Solidum, R.M.; Cooper, S.; Best, C.R.; Elacio, J.; Kavanaugh, B.C.; Spelbrink, E.M.; Brown, T.L.; Nye, K.; et al. Developmental Phenotype and Quality of Life in SLC13A5 Citrate Transporter Disorder. *Developmental Medicine & Child Neurology* **2025**, *67*, 930–940, doi:10.1111/dmcn.16218.
10. Cardoso-Moreira, M.; Halbert, J.; Valloton, D.; Velten, B.; Chen, C.; Shao, Y.; Liechti, A.; Ascenção, K.; Rummel, C.; Ovchinnikova, S.; et al. Gene Expression across Mammalian Organ Development. *Nature* **2019**, *571*, 505–509, doi:10.1038/s41586-019-1338-5.
11. Langfelder, P.; Horvath, S. WGCNA: An R Package for Weighted Correlation Network Analysis. *BMC Bioinformatics* **2008**, *9*, 559, doi:10.1186/1471-2105-9-559.
12. Bakhtiarizadeh, M.R.; Hosseinpour, B.; Shahhoseini, M.; Korte, A.; Gifani, P. Weighted Gene Co-Expression Network Analysis of Endometriosis and Identification of Functional Modules Associated With Its Main Hallmarks. *Front Genet* **2018**, *9*, 453, doi:10.3389/fgene.2018.00453.
13. Li, J.; Zhou, D.; Qiu, W.; Shi, Y.; Yang, J.-J.; Chen, S.; Wang, Q.; Pan, H. Application of Weighted Gene Co-Expression Network Analysis for Data from Paired Design. *Sci Rep* **2018**, *8*, 622, doi:10.1038/s41598-017-18705-z.
14. Benjamini, Y.; Hochberg, Y. Controlling the False Discovery Rate: A Practical and Powerful Approach to Multiple Testing. *Journal of the Royal Statistical Society. Series B (Methodological)* **1995**, *57*, 289–300.
15. Dolgalev, I. Msigdbr: MSigDB Gene Sets for Multiple Organisms in a Tidy Data Format 2025.
16. Langfelder, P.; Horvath, S. Fast R Functions for Robust Correlations and Hierarchical Clustering. *Journal of Statistical Software* **2012**, *46*, 1–17, doi:10.18637/jss.v046.i11.
17. Hu, T.; Huang, W.; Li, Z.; Kane, M.A.; Zhang, L.; Huang, S.-M.; Wang, H. Comparative Proteomic Analysis of SLC13A5 Knockdown Reveals Elevated Ketogenesis and Enhanced Cellular Toxic Response to Chemotherapeutic Agents in HepG2 Cells. *Toxicol Appl Pharmacol* **2020**, *402*, 115117, doi:10.1016/j.taap.2020.115117.
18. Kopel, J.J.; Bhutia, Y.D.; Sivaprakasam, S.; Ganapathy, V. Consequences of NaCT/SLC13A5/mINDY Deficiency: Good versus Evil, Separated Only by the Blood–Brain Barrier. *Biochemical Journal* **2021**, *478*, 463–486, doi:10.1042/BCJ20200877.

 doi:10.20944/preprints202601.0041.v1

19. Rigby, M.J.; Orefice, N.S.; Lawton, A.J.; Ma, M.; Shapiro, S.L.; Yi, S.Y.; Dieterich, I.A.; Frelka, A.; Miles, H.N.; Pearce, R.A.; et al. SLC13A5/Sodium-Citrate Co-Transporter Overexpression Causes Disrupted White Matter Integrity and an Autistic-like Phenotype. *Brain Commun* **2022**, *4*, fcac002, doi:10.1093/braincomms/fcac002.
20. Fernandez-Fuente, G.; Overmyer, K.A.; Lawton, A.J.; Kasza, I.; Shapiro, S.L.; Gallego-Muñoz, P.; Coon, J.J.; Denu, J.M.; Alexander, C.M.; Puglielli, L. The Citrate Transporters SLC13A5 and SLC25A1 Elicit Different Metabolic Responses and Phenotypes in the Mouse. *Commun Biol* **2023**, *6*, 926, doi:10.1038/s42003-023-05311-1.
21. Inoue, K.; Zhuang, L.; Ganapathy, V. Human Na+ -Coupled Citrate Transporter: Primary Structure, Genomic Organization, and Transport Function. *Biochem Biophys Res Commun* **2002**, *299*, 465–471, doi:10.1016/s0006-291x(02)02669-4.
22. Inoue, K.; Zhuang, L.; Maddox, D.M.; Smith, S.B.; Ganapathy, V. Structure, Function, and Expression Pattern of a Novel Sodium-Coupled Citrate Transporter (NaCT) Cloned from Mammalian Brain. *J Biol Chem* **2002**, *277*, 39469–39476, doi:10.1074/jbc.M207072200.
23. Yodoya, E.; Wada, M.; Shimada, A.; Katsukawa, H.; Okada, N.; Yamamoto, A.; Ganapathy, V.; Fujita, T. Functional and Molecular Identification of Sodium-Coupled Dicarboxylate Transporters in Rat Primary Cultured Cerebrocortical Astrocytes and Neurons. *Journal of Neurochemistry* **2006**, *97*, 162–173, doi:10.1111/j.1471-4159.2006.03720.x.
24. Milosavljevic, S.; Glinton, K.E.; Li, X.; Medeiros, C.; Gillespie, P.; Seavitt, J.R.; Graham, B.H.; Elsea, S.H. Untargeted Metabolomics of Slc13a5 Deficiency Reveal Critical Liver–Brain Axis for Lipid Homeostasis. *Metabolites* **2022**, *12*, 351, doi:10.3390/metabo12040351.
25. Capossela, S.; Muzio, L.; Bertolo, A.; Bianchi, V.; Dati, G.; Chaabane, L.; Godi, C.; Politi, L.S.; Biffo, S.; D'Adamo, P.; et al. Growth Defects and Impaired Cognitive-Behavioral Abilities in Mice with Knockout for Eif4h, a Gene Located in the Mouse Homolog of the Williams-Beuren Syndrome Critical Region. *Am J Pathol* **2012**, *180*, 1121–1135, doi:10.1016/j.ajpath.2011.12.008.
26. Parenti, I.; Rabaneda, L.G.; Schoen, H.; Novarino, G. Neurodevelopmental Disorders: From Genetics to Functional Pathways. *Trends Neurosci* **2020**, *43*, 608–621, doi:10.1016/j.tins.2020.05.004.
27. Russ, J.B.; Stone, A.C.; Maney, K.; Morris, L.C.; Wright, C.F.; Hurst, J.H.; Cohen, J.L. Cell-Specific Expression Biases in Human Cortex of Genes Associated with Neurodevelopmental Disorders. *Sci Rep* **2025**, *15*, 23172, doi:10.1038/s41598-025-05117-7.
28. Zheng, Z.; Guo, S.; Tam, H.Y.; Wang, J.; Rao, Y.; Hui, M.-N.; Cheung, M.P.L.; Leung, A.W.L.; Wong, K.K.W.; Sharma, R.; et al. Determination of Trunk Neural Crest Cell Fate and Susceptibility to Splicing Perturbation by the DLC1-SF3B1-PHF5A Splicing Complex. *Nat Commun* **2025**, *16*, 6718, doi:10.1038/s41467-025-62003-6.
29. Rajan, A.; Fame, R.M. Brain Development and Bioenergetic Changes. *Neurobiol Dis* **2024**, *199*, 106550, doi:10.1016/j.nbd.2024.106550.
30. Bao, Y.; Hudson, Q.J.; Perera, E.M.; Akan, L.; Tobet, S.A.; Smith, C.A.; Sinclair, A.H.; Berkovitz, G.D. Expression and Evolutionary Conservation of the Tescalcin Gene during Development. *Gene Expr Patterns* **2009**, *9*, 273–281, doi:10.1016/j.gep.2009.03.004.
31. Martínez de Arrieta, C.; Pérez Jurado, L.; Bernal, J.; Coloma, A. Structure, Organization, and Chromosomal Mapping of the Human Neurogranin Gene (NRGN). *Genomics* **1997**, *41*, 243–249, doi:10.1006/geno.1997.4622.
32. Perera, E.M.; Bao, Y.; Kos, L.; Berkovitz, G. Structural and Functional Characterization of the Mouse Tescalcin Promoter. *Gene* **2010**, *464*, 50–62, doi:10.1016/j.gene.2010.06.002.
33. De Blasi, A.; Conn, P.J.; Pin, J.; Nicoletti, F. Molecular Determinants of Metabotropic Glutamate Receptor Signaling. *Trends Pharmacol Sci* **2001**, *22*, 114–120, doi:10.1016/s0165-6147(00)01635-7.
34. Jin, S.; Chen, X.; Yang, J.; Ding, J. Lactate Dehydrogenase D Is a General Dehydrogenase for D-2-Hydroxyacids and Is Associated with D-Lactic Acidosis. *Nat Commun* **2023**, *14*, 6638, doi:10.1038/s41467-023-42456-3.

 doi:10.20944/preprints202601.0041.v1

35. Kitano, J.; Yamazaki, Y.; Kimura, K.; Masukado, T.; Nakajima, Y.; Nakanishi, S. Tamalin Is a Scaffold Protein That Interacts with Multiple Neuronal Proteins in Distinct Modes of Protein-Protein Association. *J Biol Chem* **2003**, *278*, 14762–14768, doi:10.1074/jbc.M300184200.
36. Lv, G.; Sayles, N.M.; Huang, Y.; Mancinelli, C.; McAvoy, K.; Shneider, N.A.; Manfredi, G.; Kawamata, H.; Eliezer, D. Amyloid Fibril Structures Link CHCHD10 and CHCHD2 to Neurodegeneration. *Nat Commun* **2025**, *16*, 7121, doi:10.1038/s41467-025-62149-3.
37. Svichar, N.; Waheed, A.; Sly, W.S.; Hennings, J.C.; Hübner, C.A.; Chesler, M. Carbonic Anhydrases CA4 and CA14 Both Enhance AE3-Mediated Cl--HCO3- Exchange in Hippocampal Neurons. *J Neurosci* **2009**, *29*, 3252–3258, doi:10.1523/JNEUROSCI.0036-09.2009.
38. Xie, Q.; Lin, T.; Zhang, Y.; Zheng, J.; Bonanno, J.A. Molecular Cloning and Characterization of a Human AIF-like Gene with Ability to Induce Apoptosis. *J Biol Chem* **2005**, *280*, 19673–19681, doi:10.1074/jbc.M409517200.
39. Zhao, Q.; Li, J.; Feng, J.; Wang, X.; Liu, Y.; Wang, F.; Liu, L.; Jin, B.; Lin, M.; Wang, Y.; et al. Cholesterol Metabolic Reprogramming Mediates Microglia-Induced Chronic Neuroinflammation and Hinders Neurorestoration Following Stroke. *Nat Metab* **2025**, *7*, 2099–2116, doi:10.1038/s42255-025-01379-7.
40. Alaiz-Noya, M.; Miozzo, F.; Fuentes-Ramos, M.; Machnicka, M.A.; Kurowska, M.; Herrera, M.L.; Del Blanco, B.; Ninerola, S.; Bustos-Martínez, I.; Wilczynski, B.; et al. Neuronal Type-Specific Modulation of Cognition and AP-1 Signaling by Early-Life Rearing Conditions. *Nat Commun* **2025**, *16*, 9710, doi:10.1038/s41467-025-65343-5.
41. Chan, K.T.; Creed, S.J.; Bear, J.E. Unraveling the Enigma: Progress towards Understanding the Coronin Family of Actin Regulators. *Trends Cell Biol* **2011**, *21*, 481–488, doi:10.1016/j.tcb.2011.04.004.
42. Ning, L.; Tian, L.; Smirnov, S.; Vihinen, H.; Llano, O.; Vick, K.; Davis, R.L.; Rivera, C.; Gahmberg, C.G. Interactions between ICAM-5 and B1 Integrins Regulate Neuronal Synapse Formation. *J Cell Sci* **2013**, *126*, 77–89, doi:10.1242/jcs.106674.
43. Zhu, J.-L.; Liang, X. TUBA4A: The Tale of an Unconventional Tubulin. *Cytoskeleton (Hoboken)* **2025**, doi:10.1002/cm.70044.
44. Feng, Y.; Wei, Z.-H.; Liu, C.; Li, G.-Y.; Qiao, X.-Z.; Gan, Y.-J.; Zhang, C.-C.; Deng, Y.-C. Genetic Variations in GABA Metabolism and Epilepsy. *Seizure* **2022**, *101*, 22–29, doi:10.1016/j.seizure.2022.07.007.
45. Becchetti, A.; Grandi, L.C.; Cerina, M.; Amadeo, A. Nicotinic Acetylcholine Receptors and Epilepsy. *Pharmacol Res* **2023**, *189*, 106698, doi:10.1016/j.phrs.2023.106698.
46. Talvio, K.; Minkeviciene, R.; Townsley, K.G.; Achuta, V.S.; Huckins, L.M.; Corcoran, P.; Brennand, K.J.; Castrén, M.L. Reduced LYNX1 Expression in Transcriptome of Human iPSC-Derived Neural Progenitors Modeling Fragile X Syndrome. *Front Cell Dev Biol* **2022**, *10*, 1034679, doi:10.3389/fcell.2022.1034679.
47. Smith, M.R.; Glicksberg, B.S.; Li, L.; Chen, R.; Morishita, H.; Dudley, J.T. Loss-of-Function of Neuroplasticity-Related Genes Confers Risk for Human Neurodevelopmental Disorders. *Pac Symp Biocomput* **2018**, *23*, 68–79.
48. Miwa, J.M.; Stevens, T.R.; King, S.L.; Caldarone, B.J.; Ibanez-Tallon, I.; Xiao, C.; Fitzsimonds, R.M.; Pavlides, C.; Lester, H.A.; Picciotto, M.R.; et al. The Prototoxin Lynx1 Acts on Nicotinic Acetylcholine Receptors to Balance Neuronal Activity and Survival in Vivo. *Neuron* **2006**, *51*, 587–600, doi:10.1016/j.neuron.2006.07.025.
49. Gill, D.; Zagkos, L.; Gill, R.; Benzing, T.; Jordan, J.; Birkenfeld, A.L.; Burgess, S.; Zahn, G. The Citrate Transporter SLC13A5 as a Therapeutic Target for Kidney Disease: Evidence from Mendelian Randomization to Inform Drug Development 2023.
50. Zhang, L.; Hu, W.; Guo, H.; Sun, Q.; Xu, X.; Li, Z.; Qiu, Z.; Bian, J. Discovery of Highly Potent Solute Carrier 13 Member 5 (SLC13A5) Inhibitors for the Treatment of Hyperlipidemia. *J. Med. Chem.* **2024**, *67*, 6687–6704, doi:10.1021/acs.jmedchem.4c00260.
51. Akhtar, M.J.; Khan, S.A.; Kumar, B.; Chawla, P.; Bhatia, R.; Singh, K. Role of Sodium Dependent SLC13 Transporter Inhibitors in Various Metabolic Disorders. *Mol Cell Biochem* **2023**, *478*, 1669–1687, doi:10.1007/s11010-022-04618-7.
52. Brachs, S.; Winkel, A.F.; Tang, H.; Birkenfeld, A.L.; Brunner, B.; Jahn-Hofmann, K.; Margerie, D.; Ruetten, H.; Schmoll, D.; Spranger, J. Inhibition of Citrate Cotransporter Slc13a5/mINDY by RNAi Improves Hepatic

Insulin Sensitivity and Prevents Diet-Induced Non-Alcoholic Fatty Liver Disease in Mice. *Molecular Metabolism* **2016**, *5*, 1072–1082, doi:10.1016/j.molmet.2016.08.004.

53. Schumann, T.; König, J.; Henke, C.; Willmes, D.M.; Bornstein, S.R.; Jordan, J.; Fromm, M.F.; Birkenfeld, A.L. Solute Carrier Transporters as Potential Targets for the Treatment of Metabolic Disease. *Pharmacological Reviews* **2020**, *72*, 343–379, doi:10.1124/pr.118.015735.
54. Willmes, D.M.; Kurzbach, A.; Henke, C.; Schumann, T.; Zahn, G.; Heifetz, A.; Jordan, J.; Helfand, S.L.; Birkenfeld, A.L. The Longevity Gene INDY (I ′m N Ot D Ead Y et) in Metabolic Control: Potential as Pharmacological Target. *Pharmacology & Therapeutics* **2018**, *185*, 1–11, doi:10.1016/j.pharmthera.2017.10.003.
55. Kopel, J.; Higuchi, K.; Ristic, B.; Sato, T.; Ramachandran, S.; Ganapathy, V. The Hepatic Plasma Membrane Citrate Transporter NaCT (SLC13A5) as a Molecular Target for Metformin. *Sci Rep* **2020**, *10*, 8536, doi:10.1038/s41598-020-65621-w.
56. Pajares, M.; Cuadrado, A.; Rojo, A.I. Modulation of Proteostasis by Transcription Factor NRF2 and Impact in Neurodegenerative Diseases. *Redox Biol* **2017**, *11*, 543–553, doi:10.1016/j.redox.2017.01.006.
57. 57. Song, Y.; Wang, W.; Wang, B.; Shi, Q. The Protective Mechanism of TFAM on Mitochondrial DNA and Its Role in Neurodegenerative Diseases. *Mol Neurobiol* **2024**, *61*, 4381–4390, doi:10.1007/s12035-023-03841-7.
58. Williams, L.M.; Lago, B.A.; McArthur, A.G.; Raphenya, A.R.; Pray, N.; Saleem, N.; Salas, S.; Paulson, K.; Mangar, R.S.; Liu, Y.; et al. The Transcription Factor, Nuclear Factor, Erythroid 2 (Nfe2), Is a Regulator of the Oxidative Stress Response during Danio Rerio Development. *Aquat Toxicol* **2016**, *180*, 141–154, doi:10.1016/j.aquatox.2016.09.019.